Received: 19 October 2022 | Revised: 23 February 2023 | Accepted: 31 May 2023

DOI: 10.1002/pip.3723

RESEARCH ARTICLE

PROGRESS IN PHOTOVOLTAICS WILEY

Offshore floating photovoltaics system assessment in worldwide perspective

S. Zahra Golroodbari | Abdulhadi W.A. Ayyad | Wilfried van Sark

Copernicus Institute of Sustainable Institute, Utrecht University, Utrecht, The Netherlands

Correspondence
S. Zahra Golroodbari, Copernicus Institute of Sustainable Institute, Utrecht University, Princetonlaan 8a, 3584CB Utrecht, The Netherlands.
Email: s.z.mirbagherigolroodbari@uu.nl

Funding information
Rijksdienst voor Ondernemend Nederland

Abstract

Floating solar photovoltaics (FPV), whether placed on freshwater bodies such as lakes or on the open seas, are an attractive solution for the deployment of photovoltaic (PV) panels that avoid competition for land with other uses, including other forms of renewable energy generation. While the vast majority of FPV deployments have been on freshwater bodies, in this paper, we chose to focus on offshore FPV, a mode of deployment that may be particularly attractive to nations where the landmass is constricted, such as is the case in small islands. There is a wide perception that sea-water cooling is the main reason for the enhanced performance of offshore FPV panels. In this paper, a worldwide assessment is made to validate this perception. To this end, a technology-specific heat transfer model is used to calculate PV system performance for a data set of 20 locations consisting of one system located on land and another one offshore. The analysis assumes that the floating offshore panels are placed on metal pontoons and that all panels are based on monocrystalline silicon technology. Our analysis shows that the energy yield difference, between land-based and offshore systems, for the time period of 2008 and 2018, varies between 20% and −4% showing that offshore FPV yield advantages are site-specific. In addition, the effect of other environmental factors, namely, irradiation level difference, ambient temperature, wind speed, precipitation, and sea surface temperature, is studied in this paper, which leads to the formulation of two different regression models. These can be used as a first step in predicting yield advantages for other locations.

KEYWORDS
climate zones, floating PV, offshore, photovoltaics, yield assessment

1 | INTRODUCTION

Solar photovoltaics (PV) presently account for roughly 28% of the total of 3.07 TW of installed renewable energy technologies,[1] a fact which reflects rapid levels of technological growth, as well as increased economic confidence with investors increasingly choosing to invest in PV installations. This is also highlighted by, among others, the World Energy Outlook 2020 published by the International Energy Agency, which dubbed solar PV as "the new king of electricity supply" within their Net Zero Emissions by 2050 scenario (NZE2050),[2] an outlook that envisages an annual installation of 500 GWp of solar PV capacity.

The annual energy yield of PV panels is determined by a number of factors. Most obviously, these include the conversion efficiency of

Wilfried van Sark, ISES member

the PV panel, which in turn is the result of the specific cell technology used (e.g., monocrystalline/polycrystalline silicon [Si], thin films based on cadmium indium gallium selenide [CIGS] or cadmium telluride [CdTe], a number of climatological/meteorological factors [irradiance, temperature], and installation details [orientation, tilt, mounting structure]). There is well-established literature covering the interplay between some climatological/meteorological factors, such as solar irradiance and temperature, and the performance of photovoltaic panels (see, e.g., Pearsall[3]). Performance variation across the globe has been correlated with Köppen–Geiger (KG) climate zones[4] for Si, CdTe, GaAs, and perovskites,[5] while recently a PV-specific KG climate classification has been suggested, which divides the globe into 12 zones based on the performance of PV panels.[6] The KG climate classification system divides the world into various regions into three separate levels. Differences across the zones are based on temperature; the amount and pattern of precipitation; and, indirectly, irradiation.[6]

Other various local effects such as dust and humidity[7] pose an additional challenge to understanding which locations across the globe are likely to have the best-performing solar PV installations. This is obviously also a question of economic importance, as the economic feasibility of any solar PV installation will be due in part to climatological considerations. A recent detailed exploration of this has been performed for mainland China, a large and ecologically/climatologically diverse landmass.[8] The authors of that paper in addition suggest that it would be most advantageous for a given electricity grid that PV installations connected to it were divided between land-based and offshore floating PV.

As a further example of increased interest in FPV, in the Netherlands, a recent roadmap for future PV deployment has shown that half of the potential can be found offshore, on the North Sea[9,10] in addition to considerable inland FPV potential as well.

While most deployments of FPV to date have been on freshwater bodies,[11] we focus in this paper on offshore FPV (OFPV). For our purposes, we include sites that are rough $\sim$ 56-km offshore from the selected port site. OFPV will be particularly attractive for small island nations, for example, Malta,[12] the Maldives,[13] and Singapore.[14] Likewise, OFPV is a particularly good option for nations with comparatively large coastal areas, such as the Netherlands.[15] In such situations, there may be no choice but to consider OFPV in order to achieve the two aims of reducing carbon emissions while maintaining energy security.

In other situations, land-based PV systems might compete with other essential demands on land use, such as agriculture, nature reserves, and recreation. Our choice of distance to offshore sites does not directly take into account factors such as wave height or the temperature differences between sites, but it is a choice aimed at ensuring a number of factors. First, based on several constraints, for example, the energy losses in electricity transmission lines as well as the possibility of building infrastructure and underwater cabling to connect an offshore PV site to an onshore connection near the port site, $\sim$ 56 km is estimated as the maximum possible distance. Second, offshore sites that are much less than 50 km away from the port would be too close to the port to give a reliable indication of differences, based on the spatial resolution of our basic dataset.[16] Finally, once a distance of 50 km is decided for the offshore site, it seemed intuitively correct to ensure that the inland sites we studied were equidistant from the port, thus ensuring consistency across our set of sites.

It is straightforward to see that deploying OFPV will offer advantages in certain contexts. While there has been immense progress made in this field in recent years,[17] economic obstacles may hamper the further deployment of OFPV.[18,19] To put this into a quantitative context, a recent review paper[20] suggests that the total cumulative capacity of FPV amounts to a marginal 2.6 GW and is concentrated in three countries (cf. the widely reported 270 GW of solar PV, which was installed worldwide in 2022). Consequently, it is important to understand exactly which sites globally can expect to have the most pronounced advantage for the use of OFPV, and these would then become the sites at which further exploration becomes feasible at first.

More recently, detailed performance data on FPV comes from the Singapore Tengah Reservoir,[14] in which the performance of eight different commercially available FPV technologies are tested. Rigorous testing from this site has allowed for a comparison of the performance of different panel technologies on FPV structures, and in particular how different PV technologies perform when used in FPV installations. Some of the main findings from this test bed include that ambient temperatures over water are typically 2–3° C lower than on land, and wind speeds over the water body are also generally higher.[14] As humidity above water is also relatively higher, the heat flux on the floating system location is decreased.

Some literature exists on the performance benefits of OFPV compared with conventional, land-based PV systems. An early overview of FPV designs provided estimates of $\sim$ 10% larger energy yields compared with similar installations on land,[19] which is explained by the cooling effect of the underlying water body leading to lower PV module temperatures. There is also another thermal modeling based on fish farm floater technology which concluded relatively different results than the earlier studies. This research conducted by a group of researchers in Norway[21] demonstrates that in order for any appreciable improvements to PV yield, one would need to take the site-specific water temperature into account. In this study, two adjacent PV strings were compared: One in direct contact with water and the other installed above water and there is an air gap between the back sheet and the water surface. The comparison results showed that a string directly in contact with the water body on average exhibits a 5%–7% higher energy yield than the string that was cooled by air, the results are based on experiments between the months of May and July.

Since any benefits or drawbacks from deployment on the water are dependent on both the site and the technology to be used, there is no single reference that can indicate a quantitative improvement in PV yield. In Olivera-Pinto and Stokkermans,[22] for instance, two pontoon floaters technologies are chosen. The first technology is made out of HDPE where the panels are in contact with air and the polymer material from their back sheet. The second one is based on a meshed

network galvanized steel frame where the panels are mainly in contact with air and the galvanized steel frames in a small ratio of the back sheet area. The results based on simulations in PVSyst[23] have demonstrated the energy yield advantage of 0.31%–0.46% for HDPE structure and 1.8%–2.59% for galvanized steel frame structure. This shows the energy yield advantage is mainly technology and site-specific.

As another example, an OFPV system on the west coast of Norway shows energy yield advantages of 6%–10% larger yield for a system in contact with water.[24] A theoretical study for an OFPV system with horizontally placed modules on the North Sea about 50 km off the coast showed an annual yield enhancement of $\sim$ 13% compared with a land-based system, which is due to increased offshore irradiance as well as cooling of the modules.[15] Here, it was found that the *PR* advantage is $\sim$ 4%. While weather and wind patterns have been considered, the effect of waves is found to be of limited importance. This contrasts with the case for tilted panels, where it would be expected that powerful waves could have led to dynamic variations in POA. Another theoretical study shows that energy loss to moving modules due to waves can range from 3% for medium wave intensity up to 9% for extreme wave intensity.[25] Based on the mathematical modeling of OFPV system on the North Sea, on an annual basis, we would expect that waves and their impact on the pontoons on which offshore FPV are sited would lead to variations of about 1%–2% in yield.[15]

The studies reported above show that offshore deployment of FPV has resulted in improved PV yields and that benefits are correlated with geography and meteorological conditions. While technology and the mounting type are also important, our approach aims to develop a model that neutralizes these impacts and isolates geography as a determinant factor of PV performance and the differences between offshore and onshore PV installations. Therefore, the aim of this research is to study the effect of geographical characteristics of the locations as well as the meteorological variables to find a meaningful correlation for the performance of OFPV systems. To this end, we consider 20 different locations across the globe from different continents and climate zones to simulate expected offshore performance advantages using irradiation, temperature, and relative humidity data, based on the NASA POWER database.[16]

The effect of salinity and bio-fouling on panel degradation and system efficiency are studied in Setiawan et al[26] and Suzuki et al.[27] However, due to the fact that not all of the water bodies in this study follow the same trend with respect to bio-fouling based on different water characteristics, we did not consider this important effect to prevent the complexity in this study. Moreover, for such large-scale FPV systems, the waves could be relatively damped for the panels if the modules are protected from water splashing based on waves. That is the reason we also neglect the salinity effect. The humid environment, as well as the above-mentioned parameters, could affect the speed of aging on the FPV system as discussed in detail in Zaharia et al.[28] Nonetheless, in this study, we assume that aging has a similar impact on all FPV systems in all locations which is the reason it does not have an effect on the performance difference between LBPV and FPV for each location.

The rest of the paper is organized as follows: Section 2 discusses the implemented methodology, and Section 3 presents and discusses the obtained results. Finally, in the last section, conclusions are presented.

2 | VARIABLES AND DATA ACQUISITION

Solar irradiation and ambient temperature are two key parameters in the solar PV system performance calculations. In this research, we will broaden our model by considering other variables as well, namely Atmospheric variables, climate zone, and ocean stream currents.

- **Atmospheric variables**
  Mekhilef et al[7] describe the multivariate interaction between solar irradiance, dust levels, and relative humidity to impact the performance of PV cells. Note that the influence of humidity can not be addressed without considering ambient temperature and wind speed. In Golroodbari and van Sark,[15] a so-called apparent temperature is estimated for solar cell temperature calculations and also the floating PV system performance analysis. In this research, first, we calculated the heat index, which is also known as apparent temperature. In the developed model the wind speed effect is considered in the cell temperature estimation. Both variables and their effect will be discussed in detail in this section.
- **Climate zones and site locations**
  The Köppen–Geiger climate zone typology[4] is by far the most widely used system to classify climate systems globally. This system divides the world map into different climate zones considering precipitation and temperature. It is noteworthy to mention that latitude and solar irradiance levels do not define climate. An illustration of that, the cities of Utrecht, the Netherlands, and Edmonton, Canada, have about the same latitude. While the former has climate classification within the Köppen–Geiger system of "Cfb" (an oceanic climate with warm summers), while the latter has a "Dfb" classification (hemiboreal), and its climate is more similar to Stockholm, Sweden, which is far (1450 km) to the north-east of Utrecht.
- **Ocean stream current**
  An ocean current is a continuous, directed movement of seawater generated by a number of forces acting upon the water, including wind, the Coriolis effect, breaking waves, temperature, and salinity differences. Ocean currents can be classified into two main ones: (i) Surface circulation depending on wind speed, and (ii) deep water currents or thermohaline circulation, depending on both temperature and salinity.[29] They cannot be separated by oceanographic measurements.

2.1 | Data acquisition

In this paper, we utilize a dataset based on 20 port sites across the world, which covers a wide geographical range. Each of the port cities

was geocoded using an open street map API, giving a longitude and latitude pair as well as a complete bounding box for each site (see Table 1 and Figure 1). Each coastal/port site is expanded into a site twin by adding one corresponding offshore site and one corresponding inland site. The offshore sites are generally chosen to be equidistant (56 km) from the coastal/port site. Within the twins, the bounding box for the coastal site was used to define the KG classification for them, using the hddtools package.[30] One limitation of this approach, in general, is that there is as of yet no readily available survey that classifies the open seas according to the KG system.[31]

The geocoded coordinates (Table 1) were used as the starting point from which the locations of the inland and offshore sites were determined. The following approach was taken:

1. For sites connecting to the open water toward the North, the offshore site was found by adding 0.5° to the latitude. The reverse was done for sites with open water to the South: the offshore site was found by subtracting 0.5° from the latitude. Likewise, for each triplet, the inland site was found by going in the opposite direction. The choice of 0.5° was deliberate with the intention to match the

No.	Name	Country code	Latitude (degrees)	Longitude (degrees)	Ocean current	KG class
1	Bandar Penawar	MYS	1.56N	104.23E	WS	Af
2	Ciudad del Carmen	MEX	18.65N	91.81 W	WS	Aw
3	DaNang Port	VNM	16.08N	108.22E	NA	Am
4	El Emir	URY	34.96S	54.94 W	CS	Cfb
5	Hengsha Island	CHN	31.32N	121.85E	NA	Cfa
6	Katsuura	JPN	35.16N	140.32E	CS	Cfa
7	Kwala Tanjung	IDN	3.35N	99.45E	WS	Af
8	Limassol Port	CYP	34.65N	33.016E	NA	Csa
9	Port Antonio	JAM	18.18N	76.45 W	WS	Am
10	Port Coquitlam	CAN	48.55N	124.43 W	WS	Cfb
11	Port Moresby	PNG	9.47S	147.16E	WS	Aw
12	Port of Rotterdam	NLD	51.98N	4.13E	WS	Cfb
13	Port Shepstone	ZAF	30.73S	30.45E	WS	Cfa
14	Port Vell	ESP	41.38N	2.18E	NA	Csa
15	Puerto Belgrano	ARG	38.89S	62.10 W	CS	Cfa
16	Puerto Colombia	COL	10.99N	74.96 W	WS	Aw
17	Puerto La Cruz	VEN	10.21N	64.63 W	WS	BSh
18	Ras Laffan	QAT	25.92N	51.58E	NA	BWh
19	South Golden Beach	AUS	28.50S	153.55E	CS	Cfa
20	Tanzania Port	TZA	6.82S	39.29E	WS	Aw

TABLE 1 The offshore and inland locations for a given port site are equidistant (about 56 km apart) from each of these sites. Country names relate to the three-character ISO country code, for example "PNG" is Papua New Guinea. Ocean class (current) is defined as Warm Stream; "WS," Cold Stream: "CS," not applicable: "NA". KG classification definitions can be found in Beck et al.[4]

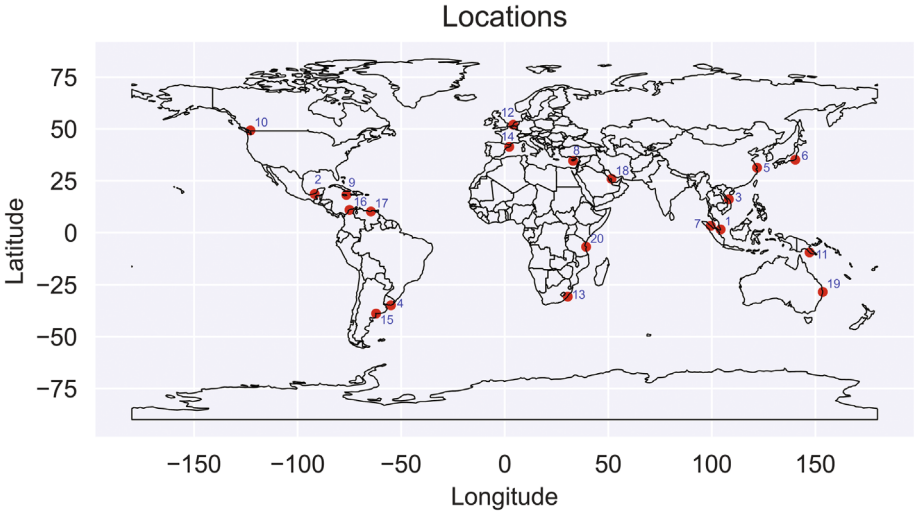

FIGURE 1 The locations of the twenty sites for this study.

level of accuracy in the downloaded data from NASA POWER[32] (see below).

2. For sites facing east or west, the longitude was modified by the equivalent of 56 km. Note that the amount of longitude variation varies with latitude: 1° longitude represents about 111 km at the Equator, but the same amount of longitudinal distance shrinks for increasing latitude when measured in kilometers to the North and South. For the data set used here, the largest (absolute) value of latitude is 51.98° (corresponding to the Dutch site), for which 56 km along the longitudinal direction is equivalent to about 0.82° longitude.

The above selection rules ensure that there is no more than 56 km between a coastal site and the OFPV site, chosen as an upper limit for the distances to ensure the feasibility of the siting.

2.2 | Meteorological data

Historical data based on satellite imagery of meteorological data for a given set of longitude and latitude coordinates are available via the NASA POWER service.[32] We used an hourly temporal resolution for 10 years of data, extending from January 2008 to January 2018. We extracted hourly averages for irradiance H (in kWh/m^2), clearness index k_T, temperature (ambient T_a and sea surface T_s), wind speed v_w, and relative humidity RH. The ambient temperatures collected for the offshore sites were the sea surface temperatures, while for the inland and coastal sites, these were the air temperatures at 2 m height. Additionally, we downloaded solar azimuths and solar hour (cosines) values in order to facilitate the transposition from direct normal irradiation (DNI) to plane-of-array.

Further discussions about the uncertainty of the meteorological data are provided in Section 4.

2.3 | Heat index

The heat index (HI) (°C) of a given combination of dry-bulb ambient temperature and relative humidity (RH) is defined as the dry-bulb temperature, which would feel the same if the water vapor pressure were 1.6 kPa.[33] The method of calculating heat index varies across environmental studies, and many different methods for calculating this metric are studied in research by Anderson et al.[34]

In this work, we used Equation (1) subject to the correction factor shown in Equation (2); the coefficients are tabulated at Table 2.[34,35]

$$\begin{aligned} HI &= a_0 + a_1 T + a_2 RH + a_3 T \times RH + a_4 T^2 + a_5 (RH)^2 \\ &\quad + a_6 T^2 \times RH + a_7 T \times (RH)^2 + a_8 T^2 \times (RH)^2 \end{aligned} \tag{1}$$

$$\{HI | T < 79^o F\} = T \tag{2}$$

where T is the ambient temperature in °F, RH is relative humidity in [%] and HI is denoting the heat index. In other words, we set the heat index to be the same as the temperature when the temperature value is below 79 (°C) Fahrenheit.

2.4 | Heat transfer

A one-dimensional heat transfer analysis model is developed in this research to calculate the solar cell temperature considering the sea surface temperature, and heat transfer in the system consisting of PV module, pontoon, and ocean water. The pontoon is assumed to be made out of steel, thus because of the good heat conductivity of steel we assumed that the temperature of the pontoon is equal to the water surface temperature at the beginning of the analysis.

As the solar panels during the day will have higher temperature compared with the pontoon and sea surface temperature, we consider the heat flux flow to go from the solar module toward the water. The equilibrium equation of the one-dimensional heat transfer analysis is defined as follows:

$$Q_{PV} = Q_{PO} \tag{3}$$

where Q_i, $i \in PV, PO$ is the heat flow rate (W/m^2), and PV and PO denote the PV module and the pontoon, respectively. The heat flow rates in Equation (3) are as follows:

$$Q_i = U_i \times A_i \times \Delta T_i \tag{4}$$

where U_i is thermal transmittance, A_i is module/pontoon area, and ΔT_i is the temperature difference.

The U value for the solar module is estimated using the same model as discussed in Sánchez-Palencia et al.[36] In this model, the U value for the module is a function of solar irradiation. After linearization of this model, we could estimate the U value for the solar modules in this model considering

$$U = \frac{G}{1500} + 2 \tag{5}$$

TABLE 2 Coefficients for the HI calculations.[34,35]

a_0	a_1	a_2	a_3	a_4	a_5	a_6	a_7	a_8
−42.4	2.05	10.14	−0.22	$-6.84\ 10^{-3}$	$-5.48\ 10^{-2}$	$1.23\ 10^{-3}$	8.5310^{-4}	-1.9910^{-6}

in which G is solar irradiance.

2.5 | Cell temperature

The efficiency of photovoltaic cells depends on the cell temperature, which is usually described by temperature coefficients for the current, the voltage, and the power. In Tina et al,[37] thermal analysis has been done considering the cooling effect of evaporation and the coefficient values introduced by Faiman[38] have been optimized based on their panel's characteristics. A similar method used in this work, which is shown in Equation (6), is a simple empirical model implemented by Koehl et al[39] to estimate the cell temperature T_{Cell}

$$T_{Cell} = T_{amb} + \frac{G}{U_0 + (U_1 \times v_w)} \tag{6}$$

where T_{amb} is ambient temperature, U_0 and U_1 are correlation coefficients (Table 3), and v_w is local wind speed near the modules.

2.6 | Energy yield

To calculate the energy yield Y for any PV system, we use

$$Y = \eta(T_{PV}, G) H (1 - L_o) \tag{7}$$

with η the efficiency of the PV panels used, which depends on PV temperature (T_{PV} [°C]) and irradiance (G [W/m^2]), H (kWh/m^2) the solar irradiation, and L_o representing losses due to system losses other than caused by temperature, and which we assume to be 10% throughout, based on typical performance ratio values found in the literature.[40] Temperature losses are accounted for in the definition of the efficiency of the PV panels, as follows[41]:

$$\eta = \eta_{STC}(1 - \beta(T_{PV} - 25) + \gamma \log_{10}(G)) \tag{8}$$

where η_{STC} is the nameplate or standard test conditions (STC[42]) efficiency of the PV panel, β and γ are material-specific properties, T_{PV} is the operating cell or panel temperature (in °C), and G is the solar irradiance (in W/m^2). We use $\eta_{STC} = 0.1935$[15] (or a 1.6 m^2 sized 310 Wp module), $\beta = 0.0045°C^{-1}$, and $\gamma = 0.12$, both for crystalline silicon,[43] and $L_o = 0.1$, based on Reich et al.[40]

We further define the absolute and relative offshore yield advantage as

$$Y_{advantage} = Y_{offshore} - Y_{inland} \tag{9}$$

$$Y_{advantage,rel} = \frac{Y_{offshore} - Y_{inland}}{Y_{inland}} \times 100 \tag{10}$$

which provides the advantage (or disadvantage) when comparing an offshore site with an inland site with >50-km distance in between.

Figure 2 shows the algorithm flowchart of the whole methodology discussed in this section to calculate the energy yield for this study. The energy yield calculated from this algorithm will be used to compare different locations in their offshore PV advantage in terms of performance.

2.7 | Regression analysis

For finding the correlation between the independent variables and the offshore PV advantage in Equation (10), two different methodologies are used: (i) Multiple linear regression (MLR) and (ii) multivariate polynomial regression (MPR). Both methods will be discussed in the following.

2.7.1 | MLR

MLR is a statistical technique that can be used to analyze the relationship between a single dependent variable and several independent variables. The objective of multiple regression analysis is to use the independent variables whose values are known to predict the value of the single dependent value. The general form of the regression equation with multiple predictors is[44]

$$\hat{y} = b_0 + \sum_{i=1}^{n} b_i x_i, i \in [1, n] \tag{11}$$

where b_0 is the intercept, and b_i is coefficient number i, n is the number of independent variables, and x_i is variable number i. The ordinary least squares (OLS) regression can be used as a method to derive the regression coefficients. This method is based on minimizing the sum of the squares of the deviations of the observed and predicted values of $\hat{y}$.

TABLE 3 Koehl correlation coefficients for different technologies.[39]

PV technology	Monocrystalline silicon (m-Si)	Polycrystalline silicon (p-Si)	Microcrystalline silicon (a-Si)	Amorphous silicon (c-Si)	Cadmium telluride (CdTe)
U_0	30.02			25.73	23.37
U_1	6.28			10.67	5.44

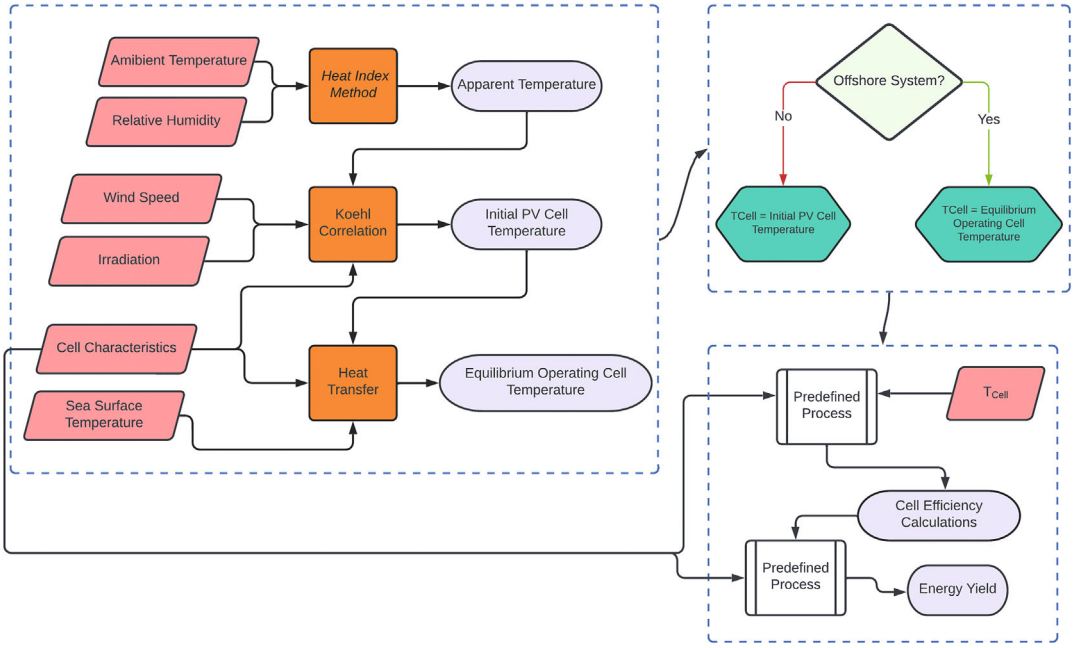

FIGURE 2 The flowchart for the described methodology to calculate the energy yield.

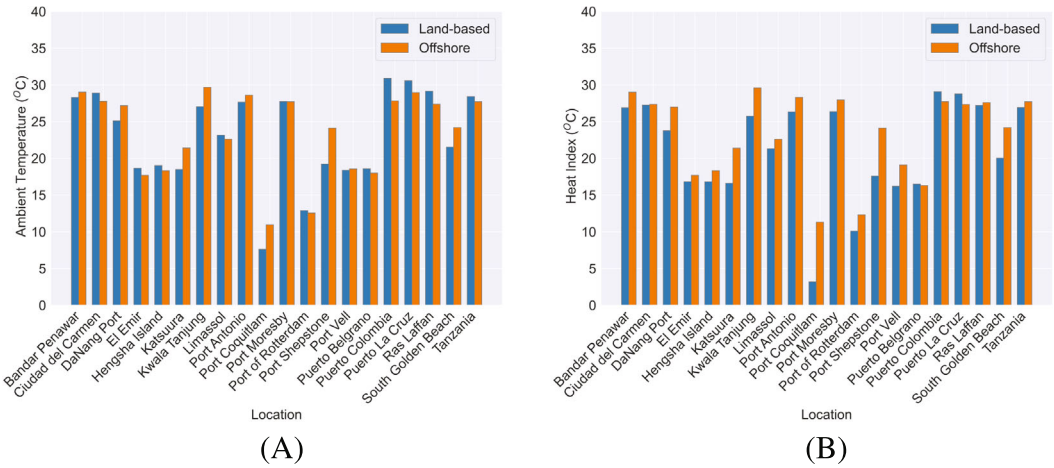

FIGURE 3 (A) Ambient temperature and (B) heat index, for all locations at both land-based and offshore system sites.

2.7.2 | MPR

The MPR model provides an effective way to describe complex nonlinear input–output relationships since it is tractable for optimization, sensitivity analysis and prediction of confidence intervals.[45] MPR for a second-order polynomial is defined in Equation (12).

$$\hat{y} = b_0 + \sum_{i=1}^{n} b_{i,1} x_i + \sum_{j=1}^{n} \sum_{i=1}^{n} b_{i,j} x_i x_j, i,j \in [1,n] \quad (12)$$

where parameters are defined as in Equation (11), noting that an additional variable j is used. In this research, the collected data are used to find a correlation between variables and the absolute and relative yield advantage. Thus, in addition to the methodology for deriving the coefficients, it is essential to define the correct independent variables. We will discuss these variables later in the following section.

3 | RESULTS AND DISCUSSIONS

In this section, the solar cell operating temperature for both offshore and land-based systems will be discussed, considering different variables, that is, wind speed, relative humidity, ambient temperature, and

sea surface temperature. Moreover, the energy yield for all 20 locations will be compared between offshore and land-based systems.

Figure 3 shows the average ambient temperature and a heat index of all locations between this research time interval. Listing is done alphabetically, as in Table 1. Due to the fact that for computing the heat index we only consider the effect of relative humidity, it is clearly shown that the heat index is not necessarily lower for the offshore system. However, we should take into consideration that ambient temperature and heat index are not the only parameters relevant to the performance of offshore systems.

3.1 | Operating temperature for modules

Figure 4A shows the average operating cell temperature for all locations for both offshore and land-based PV systems. The analysis of temperature differences between offshore and inland sites for the different locations showed that in almost all of the cases, the module temperatures at offshore sites were lower compared with the land-based sites which is the result of the water cooling effect for this specific FPV structure with steel pontoons. The average cell temperature difference is defined in Equation (13). The maximum value for this variable is 0.32°C which belongs to Port Coquitlam located in British Columbia, Canada, and the minimum value is −14°C belonging to Puerto Colombia located in Atlántico Department, Colombia.

$$\Delta T_{Cell} = T_{Offshore} - T_{Land-based} \tag{13}$$

The positive value for the Port Coquitlam site is a result of the effect of the Alaska Current. This is a southwestern shallow warm-water current alongside the west coast of the North American continent beginning at about 48–50°N, which is quite close to the location of the site. It has been mentioned by Walsh et al[46] that due to the high latitude marine heat wave in 2016, the Gulf of Alaska (GOA) and the Bering Sea have been anomalously warm for several years with the heat peaking in 2016.

These years are within the time range of our data set. These temperature variations will have an effect on the sea surface temperature and, as a result, will affect the equilibrium operating cell temperature as well.

However, the condition is different for the Puerto Colombia site. The large difference between the land-based and offshore temperature is also discussed in Ortiz-Royero et al.[47]: Strong outbreak of cold air from the north called "northers" not only brings the sea surface and ambient temperature on the offshore side down but also may cause gales and very strong waves toward the coastal areas.[48]

Figure 5 shows different temperatures, namely, apparent temperature (*HI*), sea surface temperature, cell temperature only with wind cooling effect (initial temperature), and final equilibrium operating cell temperature. Although the average sea surface temperature in most of the locations is higher than the *HI*, shown in Figure 5A, the water cooling effect is clearly shown in Figure 5B, and for all of the locations, the average of the final cell temperature is lower than its initial value.

3.2 | Yield advantage

In order to calculate the energy yield advantage, we use the equivalent of 1 MWp of panels. For this, an area of about 5200 m^2 would be needed all placed horizontally on various connected pontoons assuming that we use the 310-Wp module as mentioned above. We present our results in specific annual yields of kWh/kWp. Table 4 provides the calculated energy yields for the sites within each location as well as the absolute and relative yield advantage.

The energy yields depend on irradiance and conversion efficiency, which mainly depends on the cell operating temperature which itself is a function of ambient temperature and sea surface temperature for FPV systems, and also wind speed.

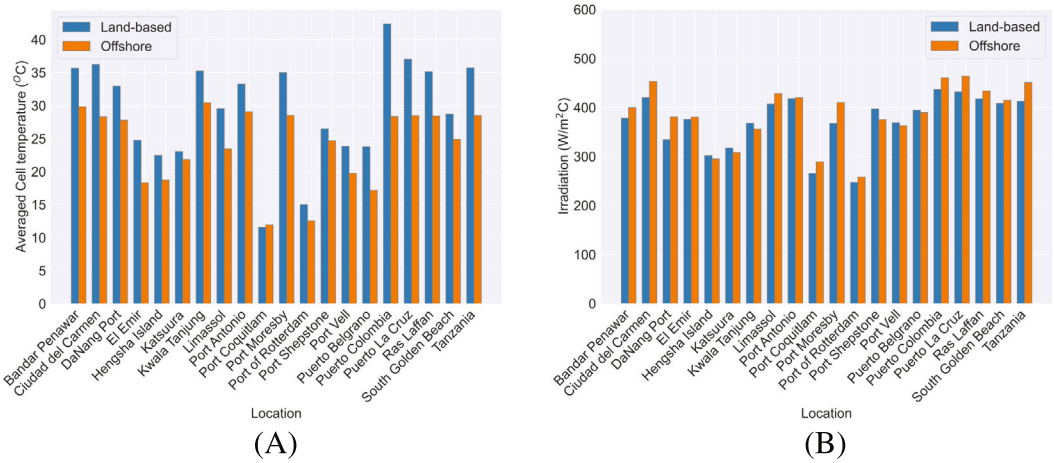

FIGURE 4 Average (A) cell temperature and (B) irradiation levels, for all locations for both offshore and inland sides.

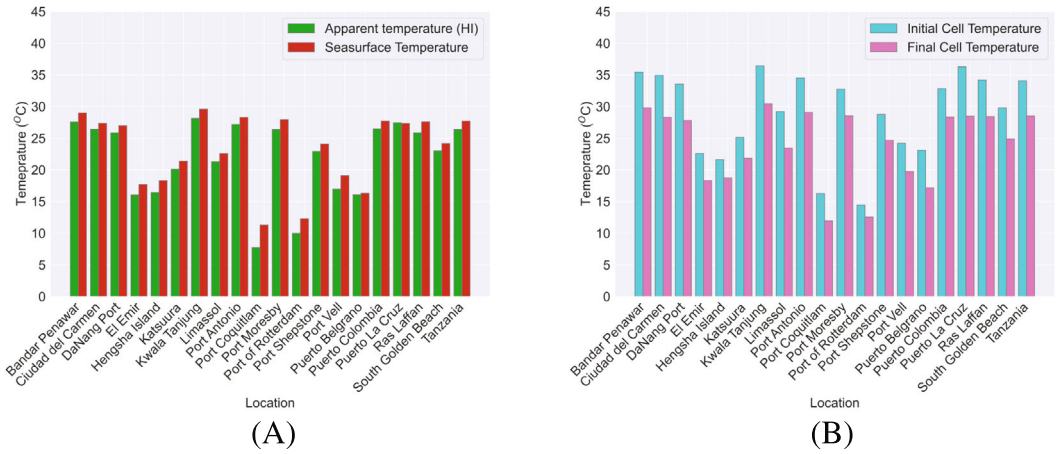

FIGURE 5 (A) Heat Index and sea surface temperature; (B) initial and final cell temperature of the offshore side for all locations between the years 2008 and 2018.

TABLE 4 Average annual yields in kWh/kWp across all locations for offshore and land-based PV systems.

No.	Site	Yield		Offshore advantage (kWh/kWp)	Relative offshore advantage (%)
		Offshore (kWh/kWp)	Inland (kWh/kWp)		
1	Bandar Penawar	1658.65	1514.35	144.30	9.53
2	Ciudad del Carmen	1899.62	1677.71	221.90	13.22
3	DaNang Port	1589.96	1328.50	261.45	19.68
4	El Emir	1639.97	1549.98	89.99	5.80
5	Hengsha Island	1259.64	1263.69	−4.05	−0.32
6	Katsuura	1304.28	1321.14	−16.86	−1.27
7	Kwala Tanjung	1472.17	1484.61	−12.44	−0.83
8	New Limassol Port	1818.66	1654.61	164.05	9.91
9	Port Antonio	1750.85	1699.01	51.84	3.05
10	Port Coquitlam	1255.03	1115.08	139.95	12.91
11	Port Moresby	1711.61	1469.96	241.64	16.43
12	Port of Rotterdam	1117.90	1037.93	79.97	7.70
13	Port Shepstone	1584.99	1646.81	−61.81	−3.84
14	Port Vell	1550.65	1521.49	29.15	1.91
15	Puerto Belgrano	1681.68	1632.73	48.94	2.99
16	Puerto Colombia	1932.02	1700.09	231.91	13.64
17	Puerto La Cruz	1943.69	1727.55	216.13	12.51
18	Ras Laffan	1811.22	1677.09	134.13	7.99
19	South Golden Beach	1752.98	1668.95	84.03	5.03
20	Tanzania Port	1889.43	1653.09	236.33	14.29

Note: The colored values in the table belong to the locations with negative advantage of the offshore system.

To have a better understanding of the energy yield tabulated in Table 4, let us first discuss the irradiation level difference for the locations and between the sites. Figure 4B shows the average irradiation during the period of this study for all locations and sites. In 70% of the locations, the average value for irradiation at the offshore site is higher than at the land-based site. The maximum and minimum irradiation level difference between the land-based and offshore systems are found for the DaNang Port and Port Shepstone sites, which is 13.94% and −5.42%, respectively.

Although 30% of the locations show a relatively lower average irradiation level on the offshore sites, the temperate difference compensation leads to an increase in energy yield of some of the sites: Only 20% of the locations show a negative energy yield difference. For instance, at the Port Vell site, although the irradiation level

difference is −1.71%, the energy yield difference is 1.91%, which is indicating that the offshore PV system performs relatively better for this location in comparison with the land-based PV system.

Considering the data in Table 4, we would like to compare the two best and two worst case results for the energy yield advantage, namely, DaNang port and Port Moresby as two higher values and Port Shepstone and Katsuura as two lower cases. Figure 6 shows the scatter plots of energy yield versus irradiation for each location. For the two best locations, not only the irradiation level is much higher for the offshore side but also the slope of the scatter plot of energy yield versus irradiation is bigger. For the other two locations, the scatter plots for land-based and offshore sides are almost similar, which means that in terms of energy yield, the offshore system does not have a better performance compared with the land-based system.

Figure 7 shows the final cell temperature versus the fluid temperature, which is considered as water for offshore and air for the land-based system. As shown for the two best locations the dry-bulb temperature for the land-based system is relatively higher compared with the other two locations. This means that the land-based system in the two worst-case scenarios performs better compared with the land-based systems of best case scenarios, in terms of the effect of air temperature on final cell temperature. However, the water cooling effect is much more tangible for the environments where the minimum temperature is higher.

It helps to focus on one specific location to illustrate some of the main conclusions in this paper.

We consider the case of Qatar, with latitude and longitude values as follows: coastal site 25.915°N, 51.580°E, offshore site 26.420°N, 51.580°E. Both Qatar sites have high levels of irradiance, but the offshore site receives consistently higher irradiance than the other site (see Figure 8A). Partial explanations for this include a higher level of diffuse radiation on the open seas due to, for example, cloud conditions or a relatively low level of localized pollution.

Yet, as with many of the other sites, the offshore site for Qatar shows higher apparent temperatures than the inland site. However, the water cooling effect and the higher irradiation level cause the offshore floating system performing significantly higher, and as tabulated in Table 4 the energy yield advantage is 7.99%.

Finally, let us consider the two locations with maximum and minimum temperature differences, which were named before, that is, Puerto Colombia and Port Coquitlam. Figure 9 shows some information about these two locations. Although the final cell temperature of the offshore site for Port Coquitlam is almost always a positive value, it barely exceeds 20°C. However, this value for the land-based side of this location belongs to a very wide range from very low to very high temperatures. In contrast, the final cell temperature for the offshore site of Puerto Colombia is limited and is always above 20°C. This value for the land-based site in this location is also always above 20°C

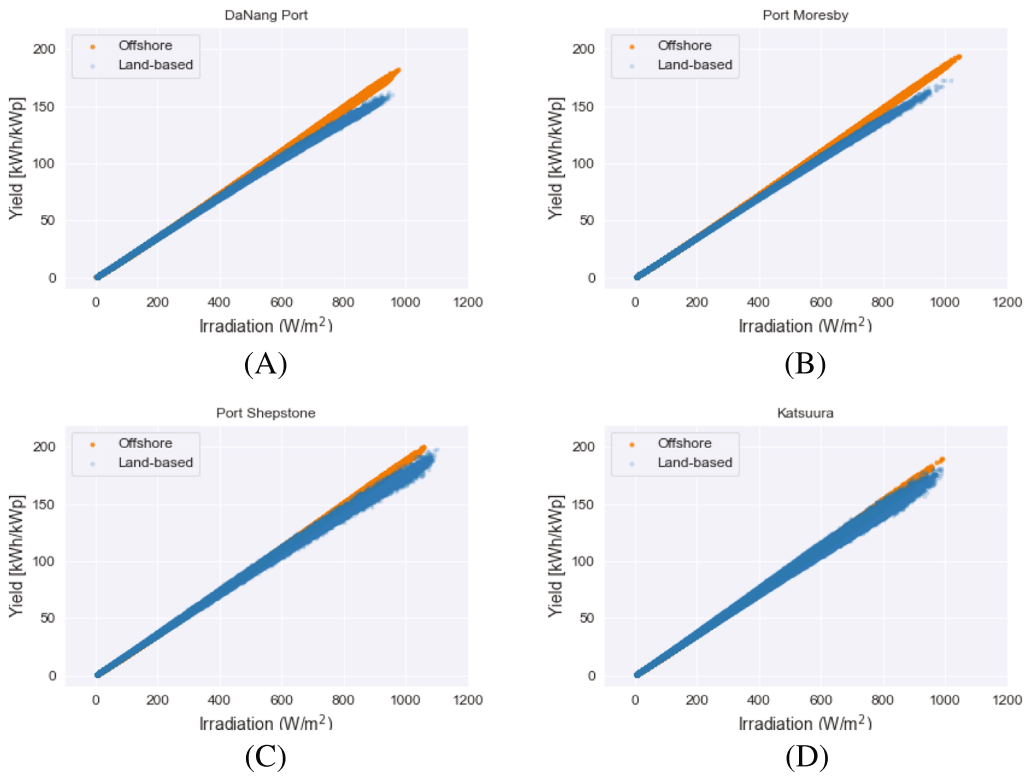

FIGURE 6 Scatter plots of energy yield versus irradiation level in hourly time resolution for (A) DaNang Port, (B) Port Moresby, (C) Port Shepstone, (D) Katsuura.

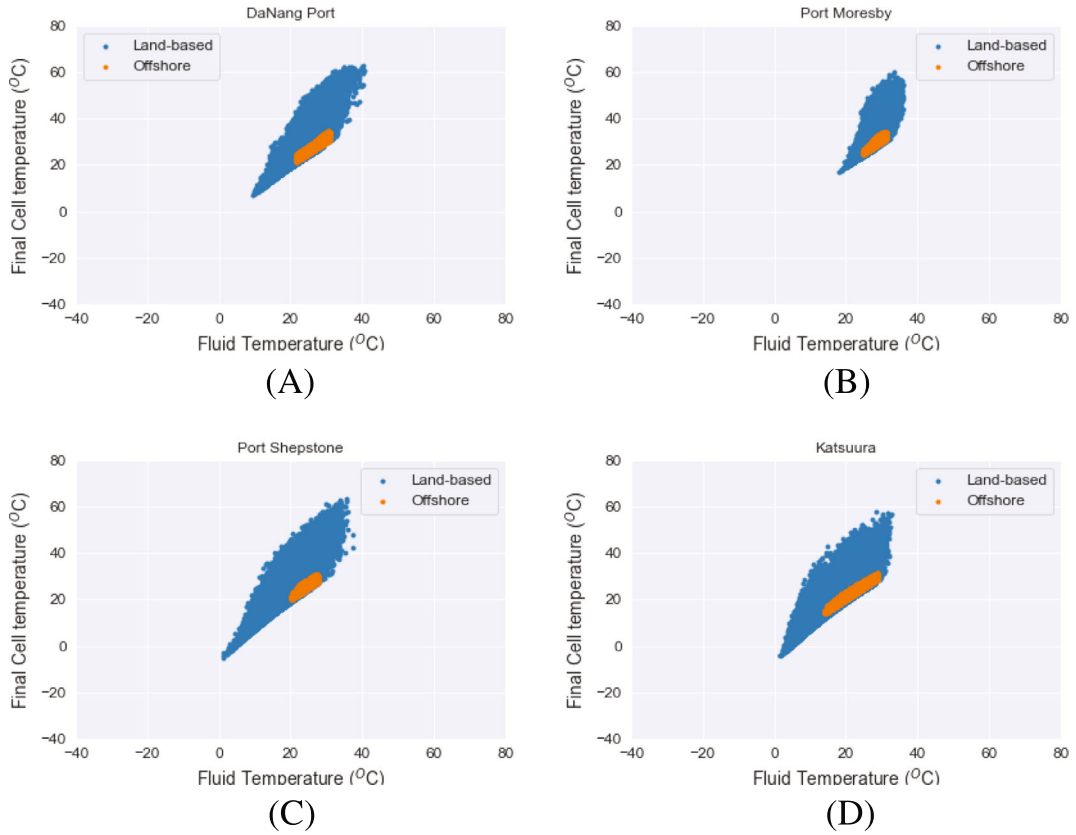

FIGURE 7 Scatter plots of final cell temperature versus ambient temperature in hourly time resolution for (A) DaNang Port, (B) Port Moresby, (C) Port Shepstone, (D) Katsuura.

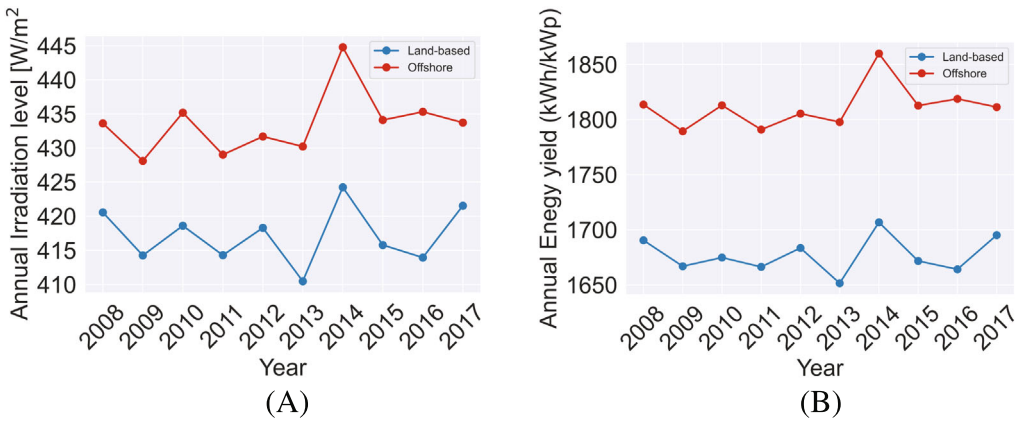

FIGURE 8 (A) Average Irradiation levels per annum and (B) annual energy yield, for Ras Laffan located at Qatar for both land-based and offshore system sites.

and PV cells could get very hot. This affects the cell efficiency, which is clearly shown in Figures 9C,D. A wide range of the final cell temperature due to the ambient condition is shown in the cell efficiency for Port Coquitlam, and it shows that the cell efficiency for the offshore system is not always better than the land-based for this location. Energy yield for Port Coquitlam is 12.9% higher, as also shown in Table 4, the average irradiation level is higher at the offshore site for this location also and the effect of temperature difference is counted. However, the energy yield difference for Puerto Colombia is 13.64%, which is mainly the effect of temperature difference.

3.3 | Regression analysis

Having studied the performance difference between land-based and offshore systems, we will discuss how we can find a reliable

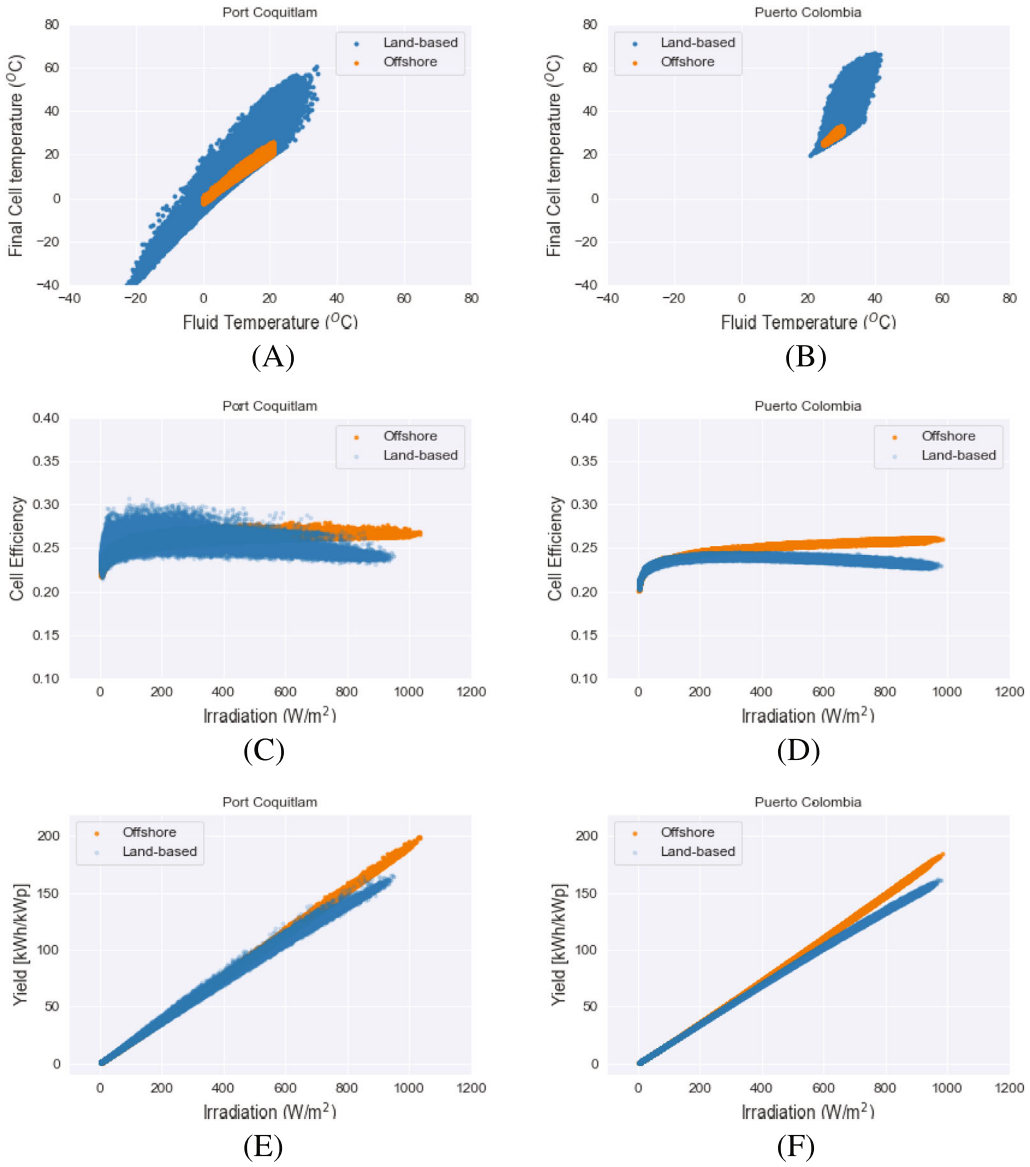

FIGURE 9 Scatter plots of (A,B) final cell temperature versus fluid temperatures, namely, water and air, (C,D) cell efficiency versus irradiation, (E,F) energy yield versus irradiation in hourly time resolution for Port Coquitlam and Puetro Colombia.

correlation between the offshore yield advantage defined in Equation (10) and the environmental variables. To this end, first, we need to define the independent variables and thereafter develop the two regression methods, that is, (i) MLR and (ii) MPR. We will analyze the accuracy of the model by calculating the metrics R^2 and root mean squared error (RMSE).

In the below list, we summarize the five main environmental/meteorological variables that we will examine in our regression model:

- ΔG (%)
  Equation (14) represents the difference in irradiation level between offshore (G_S) and land-based (G_L) sites.

$$\Delta G = \frac{G_S - G_L}{G_L} \times 100 \tag{14}$$

- Pr (mm/h)
  The precipitation is expressed in average rainfall thickness per hour (mm/h). This metric is one of the important metrics in the Köppen–Geiger climate zone typology.
- T_S (°C)
  Average sea surface temperature during the study period representing either the system to be on the warm or cold stream. Due to the fact that the cold and warm streams on the sea surface may vary by the passage of time, this variable is more reliable than a

boolean variable which represents to have either a cold or warm stream on the location.

- Δv_W (%)
  Equation (15) represents the difference in wind speed between offshore ($v_{W,S}$) and land-based $v_{W,L}$ sites.

$$\Delta v_W = \frac{v_{W,S} - v_{W,L}}{v_{W,L}} \times 100 \tag{15}$$

Considering the above-mentioned independent variables, we are able to define the MLR and MPR as shown in Equation (16) and Equation (17), respectively.

$$\widehat{\Delta E_Y} = \alpha_0 + \alpha_1 \Delta G + \alpha_2 Pr + \alpha_3 T_S + \alpha_4 \Delta v_W \tag{16}$$

$$\begin{aligned}\widehat{\Delta E_Y} = {} & \beta_0 + \beta_1 \Delta G + \beta_2 Pr + \beta_3 T_S + \beta_4 \Delta v_W + \beta_5 \Delta G^2 + \beta_6 Pr^2 \\ & + \beta_7 T_S^2 + \beta_8 \Delta v_W^2 + \beta_9 \Delta G Pr + \beta_{10} \Delta G T_S + \beta_{11} \Delta G \Delta v_W + \beta_{12} Pr T_S \\ & + \beta_{13} Pr \Delta v_W + \beta_{14} T_S \Delta v_W\end{aligned} \tag{17}$$

The intercept and coefficients of MLR and MPR methods are shown in Tables 5 and 6, respectively. In addition to the coefficients, the R-squared shown as R^2 and root mean square error (RMSE) values for both methods are also calculated and listed in the tables.

Although the MPR method is much more complex, it leads to a higher R^2 compared with the MLR method. This means that the data MPR method fitted the data better compared with the MLR method. However, it should also be taken into consideration that the MPR method is very sensitive to outliers, thus the presence of outliers could affect the performance of the model. For RMSE, this is the other way around, representing that the standard deviation of the residuals is smaller for the MPR method. Residuals indicate how far the estimated points are from the real data, and RMSE shows how these residuals diverge.

One way to demonstrate the validity of the main results is that different multivariable regression methods return relatively big R-squared values. R-squared is a measure of how closely the data in a regression line fit the data in the sample. The closer the R-squared value is to 1, the better the fit. Both methods lead to good fits, as is also evident from Figure 10.

One example that shows latitude cannot by itself play a key role in this prediction is a simple comparison between Ciudad del Carmen (18.65°N, 91.80°W) and Port Antonio (18.17°N, 76.44°W). These two ports are located with more or less similar distances to the Equator, but the average energy yield advantage for Ciudad del Carmen is 13.22% while it is 3.05% for Port Antonio. This difference can be explained by investigating which variable plays the most important role in this comparison. To this end, we first consider the average sea surface temperature and the average wind speed for both locations.

Although the presented regression model has a high level of accuracy, this should not be taken as the model for a person to decide whether or not offshore FPV is definitely a feasible option for a given location. Instead, the model could be one tool of many to help focus attention on the correct geographic and climatological factors that determine the viability of offshore FPV.

3.3.1 | Sensitivity of models

One way to study the sensitivity of a function is to use partial derivatives with respect to the independent variables. Thus, model sensitivity called "M_{Sen}" can be defined as in Equation (18).

$$M_{Sen}|\theta = \frac{\partial \widehat{\Delta E_Y}}{\partial \theta} \tag{18}$$

where θ is the independent variable in the aforementioned models.

Considering Equation (18), sensitivity of the MLR model, Equation (18) can be expressed in terms of its coefficients for each variable, as MLR is a linear model. From the data in Table 5, it is clear that MLR has the highest sensitivity to precipitation, representing Köppen–Geiger climate classification and the second variable which makes the highest sensitivity is the difference of irradiation level between offshore and land-based systems.

TABLE 5 Coefficients and metrics for MLR model.

α_0	α_1	α_2	α_3	α_4	R^2	RMSE
2.4494	1.1271	−5.4096	0.0496	0.3629	0.9792	0.8972

TABLE 6 Coefficients and metrics for MPR model.

β_0	β_1	β_2	β_3	β_4	β_5
4.7643	0.9415	−41.386	0.2562	−0.4946	−1.8310e−3
β_6	β_7	β_8	β_9	β_{10}	β_{11}
18.9158	−1.3257e−2	2.4814e−1	−0.7400	2.1005e−2	−4.9547e−2
β_{12}	β_{13}	β_{14}	R^2	RMSE	
1.7674	−3.3123	−3.6208e−3	0.9927	0.5295	

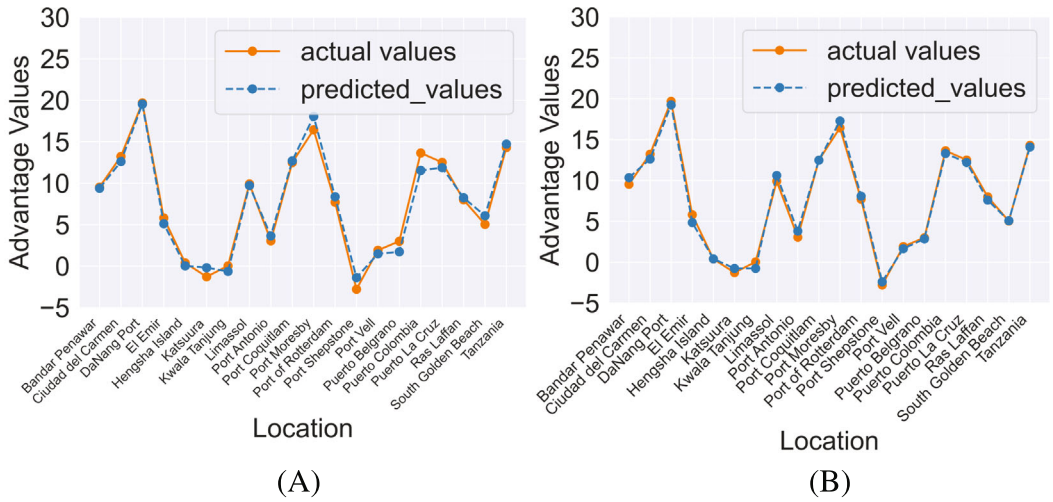

FIGURE 10 Comparison between prediction values versus actual values implementing (A) the MLR and (B) the MPR method.

To have a fair comparison for the sensitivity, the sensitivity function for the MPR model with respect to precipitation and irradiation level difference is derived and shown in Equations (19) and (20).

$$M_{Sen}|P_r = \frac{\partial \widehat{\Delta E_Y}}{\partial P_r} = \beta_2 + 2\beta_6 P_r + \beta_9 \Delta G + \beta_{12} T_S + \beta_{13} \Delta v_W \quad (19)$$

$$M_{Sen}|\Delta G = \frac{\partial \widehat{\Delta E_Y}}{\partial \Delta G} = \beta_1 + 2\beta_5 \Delta G + \beta_9 \Delta P_r + \beta_{10} T_S + \beta_{11} \Delta v_W \quad (20)$$

Considering the values for the coefficients in Table 6, we can conclude that this model similar to MLR is more sensitive to variation in precipitation than would otherwise be expected. It is important to interpret this result correctly: Specifically, it means that differences in precipitation between offshore and onshore sites—which we take to be a proxy for the KG climate classification—can suffice to explain a large part of the difference in performance between land-based and offshore PV systems. Equally important, this is also a predictive model, which avoids the direct use of the KG climate classification system but which instead can use another geography- and climate-related metrics to determine where deploying PV panels offshore would (or would not) be favorable.

4 | DISCUSSION

4.1 | Locations and dataset

For each location, the offshore FPV pontoons are located ~ 56 km away from the associated coastal site. This decision was to overcompensate for a potential lack of accuracy in the data: Since the data provided by NASA POWER have an accuracy that does not go beyond 0.5° latitude or longitude, the decision was made to ensure that all sites are at least 0.5° apart which translates to roughly 56 km.

For the sake of practicality, the number of locations is limited to 20, producing data for a total of 40 sites. Although these cover a reasonable extent of the globe, it remains possible that expanding the data set to include a greater number of locations could lead to as-yet unclear trends/relationships becoming apparent.

4.2 | Validity of data

Ultimately, the validity of the results presented here is based on the validity of NASA's Modern-Era Retrospective analysis for Research and Applications Version 2, or MERRA-2. MERRA-2 dates back to 1980 and is based on microwave radiation images. Each image is based on data collected over three hours and fitted onto a map with a 0.5-degree resolution, roughly equivalent to 50 km in the latitudinal directions (hence, the choice of 50 km when deciding the distance between offshore, coastal, and inland sites). The intensity of microwave radiation levels allows for the interpolation of solar insolations and temperatures; wind speeds are likewise calculated. A full description of the MERRA-2 project is available in review form in a paper by Geralo and co-authors.[49] Notably, the NASA POWER dataset is freely available for use and covers the entire globe, so a spatial resolution of 5˜0 km is a fairly reasonable compromise.

Throughout this paper, we sought to limit and understand the sources of the inaccuracy of the data sources in question. NASA POWER data purports also to give "optimal radiation" for tilted panels, yet, at the time of writing, the reliability of the model which produces optimal insolation could not be guaranteed for arbitrary locations.[50] Our choice of GHI radiation was thus aimed at reducing at least one important source of uncertainty. It also implies a limitation on our paper, in that we can consider only horizontally tilted panels. This excludes the studying of panels that are tilted to capture optimal levels of solar insolation; allowing for optimization of tilt panels would change the workings of this paper.

A small number of papers mostly focused on agricultural production have attempted to define the limits of the accuracy of NASA POWER's data, mostly by seeking to cross-validate the information from ground-based satellites. For example, Sayago and co-authors validated NASA POWER's solar radiation estimates against ground weather measurements across central Spain.[51] The authors report that, even in the worst cases, the value of R^2, the coefficient of determination, was no less than 0.85. Likewise, the same study reports an RMS error of $1.78\frac{MJ}{d*m^2}$ on a daily basis, or roughly equivalent to about 180 kWh per year. This suggests that high-insolation sites would be less affected than those which receive relatively less solar insolation. Bai and co-authors[52] verify NASA satellite data in China and found the solar radiation data derived from NASA POWER to be generally reliable for use when modeling maize crop yields, while the same authors reported that the NASA POWER data tended to underestimate the air temperatures. Our own adjustment of the temperature (see Section 2.2) accounts at least partly for this loss. Clearly, NASA POWER comes with its set of shortcomings and is likely to impact different sites unequally. Nonetheless, it remains the only truly "worldwide"[53] dataset, which provides all of the meteorological data which we could have needed. As a preliminary effort before further research is conducted, we judge NASA POWER to be sufficient for our needs.

4.3 | Economics

This paper deals with determining the most favorable locations for the deployment of offshore FPV in terms of energy yield. It is also clearly possible to state, based on the results, that there are some locations on the globe for which offshore FPV is simply not the most viable option. This conclusion may come from an analysis of many different metrics. Generally, the investment and installation costs of OFPV will be higher than land-based systems, while the cost of land will be absent for floating systems. On the other hand, the open water (ocean/sea) condition could be an important metric to estimate the OFPV system CAPEX based on the necessity of specific design for the structure, mounting, mooring, and anchoring systems. However, we excluded this aspect from our analysis and it is left for future work. Although more focused on meteorological and climate/geography considerations, there is a clear economic motivation for this work as well. An economically viable OFPV system will have a yield advantage that will offset higher investment and installation costs. A recent example of a hybrid offshore wind and PV system corroborates this.[54]

Of particular economic interest to this project is the differences in the lifetimes of the different solar panels. For example, a report by Zaharia and co-authors has been able to quantify the decomposition of solar panels as a consequence of corrosion caused by salinity in (e.g.) seawater.[55] Over the course of several years, it is likely that the contact between offshore solar panels and seawater would lead the offshore solar panels to degrade more rapidly than land-based PV panels; this, in addition to the infrastructure investment required to deploy PV panels offshore will influence any possible decision to deploy PV panels offshore. This again, however, is outside of the scope of our paper as we are specifically interested in determining the extent to which geography and meteorology will shape the decision to build offshore solar PV at a specific location.

5 | CONCLUSIONS

In this paper, a detailed model has been developed that allows determining the potential yield advantage that offshore floating PV systems may have across the globe. For this model, we considered steel pontoons for all the OFPV systems and assumed that panels on land are air-cooled. We implemented our model for 20 different locations across the globe, at different climate zones. While existing literature shows considerable yield advantages, we have found that the advantage may also be negative: in specific locations, offshore floating PV has a lower annual yield than a land-based system. Based on our model the average energy yield difference considering the time period of 2008 and 2018 varies from almost 20% to −4% for different locations.

To study the effect of different variables on this energy yield advantage, we have developed two regression models that can be used to predict offshore yield differences compared with land-based systems. The major finding of this study on the energy advantage between offshore and land-based PV systems is that the energy advantage is clearly site-specific. Further, we developed a meaningful regression model which quantifies a very definite correlation between a number of geographical and meteorological values and the energy (dis)advantage of deploying PV panels offshore.

We conclude that there is no iron-clad guarantee, or any type of general "rule of thumb," that deploying PV panels on bodies of water results in an improved yield of electrical energy. Yet in cases where competition for land or the need to avoid shading from the built environment necessitates moving offshore, then the approach developed in this paper can be used to make site selections. In other words, there will be some use cases where building offshore FPV might appear promising, and in such situations, having access to a geography-based regression model such as this model will help decision-makers better understand their options.

ACKNOWLEDGMENTS

The authors would like to gratefully thank Dr. Pita Verweij for the valuable insights she gave in the pathway of this research. This work is partly financially supported by the Netherlands Enterprise Agency (RVO) within the framework of the Dutch Topsector Energy (projects Comparative assessment of PV at Sea versus PV on Land, CSEALAND, and North Sea Two, NS2).

DATA AVAILABILITY STATEMENT

The data that support the findings of this study are openly available in NASA POWER at https://power.larc.nasa.gov/data-access-viewer/.

ORCID

S. Zahra Golroodbari https://orcid.org/0000-0002-5843-0463
Wilfried van Sark https://orcid.org/0000-0002-4738-1088

REFERENCES

1. Lebedys A, Akande D, Coënt N, Elhassan N, Escamilla G, Arkhipova I, Whiteman A. *Renewable capacity statistics 2022*. IRENA; 2022.
2. International Energy Agency. *World Energy Outlook 2020*. Paris, France: International Energy Agency; 2020.
3. Pearsall N, ed. *The Performance of Photovoltaic (PV) Systems Modelling, Measurement and Assessment*. Elsevier; 2016.
4. Beck HE, Zimmermann NE, McVicar TR, Vergopolan1 N, Berg A, Wood EF. Present and future Köppen-Geiger climate classification maps at 1-km resolution. *Sci Data*. 2018;5:180214.
5. Peters IM, Buonassisi T. Energy yield limits for single junction solar cells. *Joule*. 2018;2:1160-1170.
6. Ascencio-Vásquez J, Brecl K, Topič M. Methodology of Köppen-Geiger-photovoltaic climate classification and implications to worldwide mapping of PV system performance. *Solar Energy*. 2019;191:672-685.
7. Mekhilef S, Saidur R, Kamalisarvestani M. Effect of dust, humidity and air velocity on efficiency of photovoltaic cells. *Renew Sustain Energy Rev*. 2012;16:2920-2925.
8. Hu J, Harmsen R, Crijns-Graus W, Worrell E. Geographical optimization of variable renewable energy capacity in China using modern portfolio theory. *Appl Energy*. 2019;253:113614.
9. Folkerts W, Van Sark W, De Keizer C, Van Hooff W, Van den Donker M. Roadmap PV Systemen en Toepassingen. *Technical report*, SEAC, Utrecht University, TKI Urban Energy; 2017.
10. Quax R, Londo M, van Hooff W, Kuijers T, Jaap W, van Sark W, Sinke W. Assessment of spatial implications of photovoltaics deployment policies in the Netherlands. *Solar Energy*. 2022;243:381-392.
11. World Bank. Where Sun Meets Water: Floating Solar Handbook for Practitioners. *Technical report*, The World Bank; 2019.
12. Trapani K, Millar DL. Proposing offshore photovoltaic (PV) technology to the energy mix of the Maltese islands. *Energy Convers Manag*. 2013;67:18-26.
13. Keiner D, Salcedo-Puerto O, Immonen E, et al. Powering an island energy system by offshore floating technologies towards 100% renewables: a case for the Maldives. *Appl Energy*. 2022;308:118360.
14. Liu H, Krishna V, Leung JL, Reindl T, Lu Z. Field experience and performance analysis of floating PV technologies in the tropics. *Prog Photovoltaics*. 2018;26:957-967.
15. Golroodbari SZ, van Sark W. Simulation of performance differences between offshore and land-based photovoltaic systems. *Prog Photovoltaics*. 2020;28:873-886.
16. NASA POWER. Prediction of worldwide energy resources (power) project. https://power.larc.nasa.gov
17. Rosa-Clot M, Marco Tina G, eds. *Floating PV Plants*. Academic Press; 2020.
18. Gorjian S, Sharon H, Ebadi H, Kant K, Scavo FB, Tina GM. Recent technical advancements, economics and environmental impacts of floating photovoltaic solar energy conversion systems. *J Cleaner Product*. 2021;278:124285.
19. Trapani K, Redón Santafé M. A review of floating photovoltaic installations: 2007–2013. *Prog Photovoltaics: Res Appl*. 2015;23:524-532.
20. Ghigo A, Faraggiana E, Sirigu M, Mattiazzo G, Bracco G. Design and analysis of a floating photovoltaic system for offshore installation: the case study of Lampedusa. *Energies*. 2022;15(23):8804.
21. Kjeldstad T, Lindholm D, Marstein E, Selj J. Cooling of floating photovoltaics and the importance of water temperature. *Solar Energy*. 2021;218:544-551.
22. Olivera-Pinto S, Stokkermans J. Assessment of the potential of different floating solar technologies: overview and analysis of different case studies. *Energy Convers Manag*. 2020;211:112747.
23. PVSyst. PVSyst Photovoltaic Software. 2020. http://www.pvsyst.com
24. Seij JH, Lereng IH, De Paoli P, Ogaard MB, Otnes G, Bragstad S, Bjorneklett B, Marstein E. The performance of a floating PV plant at the west coast of norway. In: Proc 36th European Photovoltaic Solar Energy Conference (EUPVSEC). Marseille, France; 2019:1763-1767.
25. Dörenkämper M, Van den Werf D, Sinapis K, De Jong M, Folkerts W. Influence of wave induced movements on the performance of floating pv systems. In: Proceedings of 36th European Photovoltaic Solar Energy Conference (EUPVSEC). Marseille, France; 2019:1759-1762.
26. Setiawan F, Dewi T, Yusi S. Sea salt deposition effect on output and efficiency losses of the photovoltaic system; a case study in Palembang, indonesia. In: J Phys: Confer Ser, Vol. 1167. IOP Publishing; 2019:12028.
27. Suzuki S, Nishiyama N, Yoshino S, et al. Acceleration of potential-induced degradation by salt-mist preconditioning in crystalline silicon photovoltaic modules. *Japanese J Appl Phys*. 2015;54(8S1):8KG08.
28. Zaharia SM, Pop MA, Chicos LA, Lancea C, Semenescu A, Florea B, Chivu OR. An investigation on the reliability and degradation of polycrystalline silicon solar cells under accelerated corrosion test. *MATERIALE PLASTICE*. 2017;54(3):466.
29. Rahmstorf S. Thermohaline circulation: the current climate. *Nature*. 2003;421(6924):699.
30. Vitolo C. hddtools: Hydrological data discovery tools. *The J Open Source Softw*. 2017;2(9):56.
31. Vittolo C. Private correspondence; 2020.
32. Sparks AH. nasapower: A NASA POWER Global Meteorology, Surface Solar Energy and Climatology Data Client for R. *The J Open Source Softw*. 2018;3(30):1035.
33. Rothfusz LP, NWS Southern Region Headquarters. The heat index equation (or, more than you ever wanted to know about heat index). Fort Worth, Texas: National Oceanic and Atmospheric Administration, National Weather Service, Office of Meteorology, 9023; 1990.
34. Anderson GB, Bell ML, Peng RD. Methods to calculate the heat index as an exposure metric in environmental health research. *Environ Health Perspect*. 2013;121(10):1111-1119.
35. Patricola CM, Cook KH. Northern African climate at the end of the twenty-first century: an integrated application of regional and global climate models. *Clim Dyn*. 2010;35(1):193-212.
36. Sánchez-Palencia P, Martín-Chivelet N, Chenlo F. Modeling temperature and thermal transmittance of building integrated photovoltaic modules. *Solar Energy*. 2019;184:153-161.
37. Tina GM, Bontempo Scavo F, Merlo L, Bizzarri F. Comparative analysis of monofacial and bifacial photovoltaic modules for floating power plants. *Appl Energy*. 2021;281:116084.
38. Faiman D. Assessing the outdoor operating temperature of photovoltaic modules. *Prog Photovoltaics: Res Appl*. 2008;16(4):307-315. doi: 10.1002/pip.813
39. Koehl M, Heck M, Wiesmeier S, Wirth J. Modeling of the nominal operating cell temperature based on outdoor weathering. *Solar Energy Mater Solar Cells*. 2011;95(7):1638-1646.
40. Reich NH, Mueller B, Armbruster A, Van Sark WGJHM, Kiefer K, Reise C. Performance ratio revisited: is PR > 90% realistic? *Prog Photovoltaics: Res Appl*. 2012;20:717-726.
41. Skoplaki E, Palyvos JA. On the temperature dependence of photovoltaic module electrical performance: a review of efficiency/power correlations. *Solar Energy*. 2009;83:614-624.
42. International Electrotechnical Committee. IEC 61215:2005, crystalline silicon terrestrial photovoltaic (PV) modules—Design qualification and type approval. *Technical report*, Geneva, International Electrotechnical Committee; 2005.
43. Notton G, Cristofari C, Mattei M, Poggi P. Modelling of a double-glass photovoltaic module using finite differences. *Appl Thermal Eng*. 2005;25:2854-2877.
44. Pace L. Multiple regression. *Beginning R*. Springer; 2012:185-199.
45. Toh K-A, Yau W-Y, Jiang X. A reduced multivariate polynomial model for multimodal biometrics and classifiers fusion. *IEEE Trans Circ Syst Video Technol*. 2004;14(2):224-233.

46. Walsh JE, Thoman RL, Bhatt US, et al. The high latitude marine heat wave of 2016 and its impacts on alaska. *Bull Am Meteorol Soc*. 2018; 99(1):S39-S43.
47. Ortiz-Royero JC, Otero LJ, Restrepo JC, Ruiz J, Cadena M. Cold fronts in the Colombian Caribbean Sea and their relationship to extreme wave events. *Nat Hazards Earth Syst Sci*. 2013;13(11):2797-2804.
48. Devis-Morales A, Montoya-Sánchez RA, Bernal G, Osorio AF. Assessment of extreme wind and waves in the Colombian Caribbean Sea for offshore applications. *Appl Ocean Res*. 2017;69:10-26.
49. Gelaro R, Mccarty W, Surez MJ, et al. The modern-era retrospective analysis for research and applications, version 2 (MERRA-2). *J Clim*. 2017;30(14):5419-5454.
50. Tindell J. Private correspondence with the NASA Langley facility; 2020.
51. Sayago S, Ovando G, Almorox J, Bocco M. Daily solar radiation from NASA-POWER product: assessing its accuracy considering atmospheric transparency. *Int J Remote Sens*. 2020;41(3):897-910.
52. Bai J, Chen X, Dobermann A, Yang H, Cassman KG, Zhang F. Evaluation of NASA satellite- and model-derived weather data for simulation of maize yield potential in China. *Agronomy J*. 2010;102(1):9-16.
53. Hall J, Hall J. Evaluating the accuracy of solar radiation data sources. Solar Data Warehouse; 2010.
54. Golroodbari SZM, Vaartjes DF, Meit JBL, Van Hoeken AP, Eberveld M, Jonker H, Van Sark WGJHM. Pooling the cable: a techno-economic feasibility study of integrating offshore floating photovoltaic solar technology within an offshore wind park. *Solar Energy*. 2021;219:65-74.
55. Marian ZS, Alin PM, Antoneta CL, Camil L, Augustin S, Bogdan F, Roxana CO. An investigation on the reliability and degradation of polycrystalline silicon solar cells under accelerated corrosion test. *Materiale Plastice*. 2017;54(3):466-472.

How to cite this article: Golroodbari SZ, Ayyad AWA, van Sark W. Offshore floating photovoltaics system assessment in worldwide perspective. *Prog Photovolt Res Appl*. 2023;31(11): 1061-1077. doi:10.1002/pip.3723